Check for updates

The missing conformer: A comprehensive rotational spectroscopy study and astronomical search of two conformers of methyl cyanoacetate

Gayatri Batra[1,2], Pablo Pinacho[1], Amanda L. Steber[1,3],
Víctor M. Rivilla[4], Jesús Martín-Pintado[4],
Izaskun Jiménez-Serra[4] and Melanie Schnell[1,2]*

[1]Deutsches Elektronen-Synchrotron DESY, Hamburg, Germany, [2]Christian-Albrechts-Universität zu
Kiel, Kiel, Germany, [3]Universidad de Valladolid, Valladolid, Spain, [4]Centro de Astrobiología (CSIC-INTA),
Madrid, Spain

We performed a comprehensive investigation of methyl cyanoacetate (MCA) using high-resolution Fourier transform rotational spectroscopy. Two low energy conformers of MCA were observed in the vibrational ground state, in selected frequency regions from 2 to 110 GHz. We report accurately determined line lists, rotational constants, centrifugal distortion constants, and nuclear quadrupole coupling constants for both conformers, as well as for several singly substituted heavy-atom isotopologues. One of the conformers was previously reported; however, the rotational transitions of the second conformer, which is newly described here, are observed to be generally more intense than the latter. The accurate predictions of rotational transitions into the millimeter-wave region can facilitate the detection of these conformers of MCA in the interstellar medium. Using the rotational spectroscopy data provided here, we searched for the two conformers of MCA in a deep and unbiased spectral survey of the molecular cloud G+0.693-0.027 located in the Galactic Center. None of the MCA conformers were detected. The upper limits for their abundances were derived with respect to the abundance of molecular hydrogen.

KEYWORDS

astrochemistry, interstellar medium, methyl cyanoacetate, rotational spectroscopy, molecular structure

Introduction

In the recent years, there has been an acceleration in the pace of detection of molecules in the interstellar medium (ISM). As of August 2022, around 270 molecules have been detected in the interstellar medium or circumstellar shells, comprising of 19 different chemical elements. The majority of these molecules have been detected using radio astronomy since the 1960s with an approximate rate of ~4 detections/year since 1968 and ~6 detections/year since 2005 (McGuire, 2022). The detection rate has increased significantly, for instance, around 45 new molecules have been detected in the last 1.5 years. Updated lists of detected molecules in space can be found in the Cologne Database for Molecular Spectroscopy[1] and on astrochymist.org[2]. This increase in the detection rate can be attributed to two factors; on the one hand, to the technical advances in the field of radio astronomy and facilities such as the Atacama Large Millimeter Array, the Green Bank Telescope or the Yebes 40 m telescopes (McGuire, 2022); and on the other hand, to the increase in laboratory-based rotational spectroscopy studies of potential molecules of astrochemical interest, which provide detailed spectroscopic parameters required for their search in the ISM. With the development of chirped-pulse Fourier transform microwave (CP-FTMW) spectrometers (Brown et al., 2006), the measurement times for broadband, high-resolution microwave spectra have become several orders of magnitude shorter than what was previously possible. Due to a combination of both factors, larger and more complex molecules are becoming targets for searches in the ISM. As a starting point for the detection of a new compound, it is useful to study derivatives of molecules which have already been detected, for example, by including additional functional groups. One of the most abundant functional groups of the molecules observed in the ISM is the cyano group ($-C\equiv N$). It is present in more than 15% of the detected molecules (McGuire, 2022). The prevalence of cyano-containing molecules can be attributed to the substantial electric dipole moment of the molecule introduced by the cyano group. Since most of the molecules are detected based on their rotational fingerprint, a large value of the electric dipole moment facilitates their observation, as the rotational transition intensities are dependent on the electric dipole moment.

Additional features, such as the observation of transitions from highly excited torsional states or splittings due to large amplitude motions, could direct towards the detection of certain classes of molecules (Biver et al., 2015; Kleiner, 2019). The internal rotation of a methyl top ($-CH_3$) is hindered by a finite three-fold potential. This induces a quantum tunneling effect, which leads to the splitting of each rotational level into a non-degenerated A state and a doubly degenerated E state. Internal rotors play an important role in the astrophysical environment. Not only do they act as unique indicators of the chemical structure of Complex Organic Molecules (COMs) (Herbst and van Dishoeck, 2009) through the observation of the A/E splitting, they also carry valuable information about the physical conditions of the surrounding environment. For example, the population of torsionally excited states of the molecules containing internal rotors can provide information on the temperature of the surrounding region (Biver et al., 2015). To date, many complex molecules with internal rotors have been identified in the ISM (Herbst and van Dishoeck, 2009), as well as in comets, meteorites and asteroids (Despois et al., 2006; Walker and Cameron, 2006; Biver et al., 2015). The millimeter wave spectra of hot cores, such as Sagittarius B2 or the Orion molecular cloud, are dominated by the rotational-torsional spectra of small molecules with internal rotors, such as methanol (CH_3OH) and methyl formate ($HCOOCH_3$). An insightful review of the spectroscopy of interstellar internal rotors is given in reference (Kleiner, 2019).

To obtain a more detailed catalog of the detected molecules in the ISM, their different low-energy conformers must be considered. The majority of the detections in the ISM are reported for the lowest energy conformer, but extending this study to other energetically accessible conformers can help to evaluate the physical and chemical environment of the detection region. Moreover, it is possible to obtain accurate column densities when all the populated conformers are included, rather than based on the presence of the lowest energy variant. This is described in detail for the case of the *trans* and *gauche* conformations of ethanol (Zuckerman et al., 1975; Pearson et al., 1997).

Methyl cyanoacetate (MCA), $NCCH_2COOCH_3$, is an excellent candidate for a future astronomical detection, as it is a derivative of an already detected molecule, methyl acetate, CH_3COOCH_3 (Tercero et al., 2013). MCA contains an ester and a cyano functional group, responsible for fine and hyperfine structure, respectively. The fine structure is due to the internal rotation of the $-CH_3$ group linked to the ester oxygen, while the hyperfine structure is generated due to nuclear quadrupole coupling, caused by the presence of a ^{14}N nucleus ($I = 1$) in the cyano part of the molecule.

MCA has been studied previously using vibrational spectroscopy in the liquid (Charles et al., 1973) and in the solid phases (Sinha and Katon, 1974) to obtain information regarding the different geometries and relative energies of the conformers. Both studies concluded the presence of more than one conformer based on several unassigned bands in the infrared spectra. Later on, a detailed infrared study was conducted to obtain more information on the lowest energy conformers by analyzing data from the vapor phase and from solutions in liquid argon (Leibowitz et al., 1991). This was followed by an in-depth

---

analysis of the vibrational features in liquid (Neta and Fausto, 1998), solution (Prasad et al., 1990), and by matrix isolation techniques (Reva et al., 2001; Reva et al., 2003). Based on the previous studies and chemical intuition, MCA can adopt four possible geometries in view of the orientation of the methyl group of the ester fragment and the cyano fragment in the *syn* or *anti* orientation with respect to the carbonyl group.

Recently, a high-resolution rotational spectroscopy study of MCA was reported for the lowest energy conformer, with insights into the internal rotation barrier for the methyl top and the nuclear quadrupole coupling constants for the ^{14}N nucleus (Gregory et al., 2021). However, all the previous vibrational spectroscopy studies and the theoretical calculations predict the presence of a second conformer with a large dipole moment of around five Debye and close in energy with respect to the first conformer.

In the present work, we report the detailed characterization of the second conformer of MCA as well as an extension of the spectral range for the first conformer up to 110 GHz using rotational spectroscopy. The comprehensive rotational spectroscopic characterization of both conformers covering a broad spectral range (2-110 GHz in selected frequency regions) can aid their detection in the ISM using the high-sensitivity radio telescopes. It also emphasizes the need of extending the observational searches not only to the lowest energy conformer but to other energetically accessible conformers as well. This can also be seen in the study reporting the interstellar detection of conformer pairs of ethyl formate (C_2H_5OCHO) (Rivilla et al., 2017) and C-cyanomethanimine (HNCHCN) (Rivilla et al., 2019), where the energy difference between their conformers is small enough for both conformers to exist in the thermodynamic equilibrium at the kinetic temperature (T_k) of the gas.

Theoretical work

To facilitate the experimental analysis, quantum-chemical calculations were performed using the ORCA program package (Neese, 2012; Neese, 2018) and Gaussian 09 program package (Frisch et al., 2013). The geometry optimization calculations for the different conformers of MCA were performed with the Gaussian 09 program (Frisch et al., 2013) employing anharmonic force fields. The set of obtained rotational constants, nuclear quadrupole coupling constants, dipole moments, and centrifugal distortion constants were used to simulate the rotational spectrum. A relaxed scan of the torsional potential was performed to obtain an initial value for the barrier height of the internal rotation motion of the methyl top. A more detailed description of the calculations is provided below.

The conformational space of MCA can be described by the possible values of two dihedral angles, θ and ϕ, given by NC-

CH_2-C=O and H_3C-O-C=O, respectively, as shown in Figure 1. As a result, four different conformations are possible for MCA, as listed in Table 1 with both functional groups, -CN and -$COOCH_3$, being in -*syn* or -*anti* arrangement with respect to the carbonyl group. Geometry optimizations and anharmonic frequency calculations for the four possible conformers of MCA were performed at the B3LYP-D3/aug-cc-pVTZ level of theory. The two lowest energy conformers (hereafter, MCA_1 and MCA_2) with an energy difference of 1.4 kJ/mol are energetically accessible under our experimental conditions. The other two conformers, MCA_3 and MCA_4, are significantly higher in energy (~30 kJ/mol and ~36 kJ/mol, respectively) with respect to the lowest energy conformer MCA_1 and hence are not expected to be observed under our experimental conditions. The computed rotational constants, dipole-moment components, and zero-point corrected relative energies are given in Table 1. The energy difference between the two lowest energy conformers computed at the B3LYP-D3/aug-cc-pVTZ level of theory is within the method uncertainty. Consequently, additional single-point energy calculations were performed using the RI-MP2/cc-pVTZ level of theory and the DLPNO-CCSD(T)/CBS extrapolation based on aug-cc-pVnZ (*n* = T,Q) calculations, with TightPNO settings on the geometries obtained with the B3LYP-D3/aug-cc-pVTZ structure optimization calculation. The energy difference between MCA_1 and MCA_2 calculated at different levels of theory is summarized in Supplementary Table S1. Interestingly, the energy difference between MCA_1 and MCA_2 decreases from 1.4 kJ/mol at the B3LYP-D3/aug-cc-pVTZ level of theory to only 0.1 kJ/mol at the DLPNO-CCSD(T)/CBS level of theory.

To obtain theoretical values of the barrier heights for the methyl top internal rotation for both of the lowest energy conformers, one-dimensional potential energy scans (PES) were performed at two different levels of theory, B3LYP-D3/aug-cc-pVTZ and MP2/aug-cc-pVTZ. In the scans, the dihedral angle H-CH_2-O-C was varied in steps of 10°. For each point, all the other parameters were relaxed and the resulting PES is given in Supplementary Figure S1. The obtained values were used as a starting point for the analysis of the experimental barrier height. The comparison of the experimental and theoretical barrier height at both levels of theory is shown in Supplementary Figure S1.

Experimental details and fitting procedure

The rotational spectrum of MCA was recorded in several frequency ranges, covering 2–26 and 75-110 GHz. Three broadband chirped-pulse Fourier transform microwave/millimeter wave (CP-FTMW) spectrometers were employed, namely, the COMPACT spectrometer (2-18 GHz) (Schmitz et al., 2012; Pérez et al., 2016; Fatima et al., 2020), the *K*-
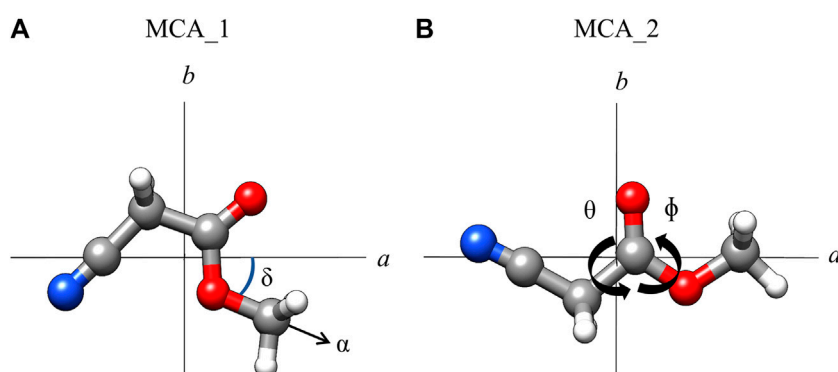
FIGURE 1
Molecular structure and principal inertial axes of MCA_1 (panel **(A)**) and MCA_2 (panel **(B)**). The c-axis is perpendicular to the ab-molecular plane. α is the methyl internal rotor axis and δ is the angle between the methyl internal rotor axis and the principal axis a. θ and ϕ are the dihedral angles. The nitrogen atoms are shown in blue, the oxygen atoms in red, the carbon atoms in grey, and the hydrogen atoms are shown in white color.

TABLE 1 Calculated parameters for the conformers of MCA at the B3LYP-D3/aug-cc-pVTZ level of theory.

Rotational parameters	MCA_1	MCA_2	MCA_3	MCA_4
A^a/MHz	5077	9509	3786	6231
B/MHz	1830	1407	2264	1624
C/MHz	1368	1244	1592	1309
$\mu_a\|\mu_b\|\mu_c{}^b$/D	−2.3/0.6/0.0	4.5/-3.0/0.0	−0.1/1.9/3.2	4.8/4.7/0.0
$\Delta E_{ZPE}{}^c$/kJ·mol^{-1}	0.0	1.4	30.4	36.0

[a] A, B, and C are the rotational constants.
[b] $\mu_a\|\mu_b\|\mu_c$ are the electric dipole-moment components.
[c] Relative zero-point.

band spectrometer (18-26 GHz) (Fatima et al., 2020), and the W-band spectrometer (75-110 GHz) (Arenas et al., 2017). For the measurements in the range of 2-26 GHz, the sample of MCA was held in a modified pulsed nozzle (Parker Series 9 valve modified to be equipped with an internal heatable reservoir) and heated at 55 °C to increase its vapor pressure. The molecular vapor was then introduced into the vacuum chamber using a supersonic expansion with 2.5 bar of neon as a backing gas. Owing to the supersonic expansion, the resulting rotational temperature goes down to $T_{rot} \approx 1$-3 K. In the W-band spectrometer, the spectrum was recorded at room temperature conditions with $T_{rot} \approx 293$ K.

The spectrum of MCA in the region between 2 and 18 GHz was recorded with the COMPACT spectrometer in three parts, 2–8, 8–13, and 13-18 GHz. The excitation chirp is generated by an arbitrary waveform generator (AWG), amplified and

transmitted into the vacuum chamber. For the 2-8 GHz region, the excitation chirp is amplified by a 300 W traveling wave tube (TWT) amplifier, while for the 8-13 GHz and 13-18 GHz regions, a 50 W solid state amplifier (SSA) is employed. These excitation pulses are then transmitted into the vacuum chamber and broadcast via a horn antenna, where a macroscopic polarization is induced when a frequency of the chirped excitation pulse is resonant with a molecular rotational transition of the sample. The relaxation of the induced macroscopic polarization of the molecular ensemble is recorded in the form of a free induction decay (FID). The spectrometer uses the fast-frame method, in which each molecular pulse is probed by a successive train of eight excitation chirps followed by recording the respective FIDs. Combined with the gas pulse repetition rate of 8 Hz, an

effective repetition rate of 64 Hz was achieved. For the 2-8 GHz experiment, four million FIDs (each collected for 40 μs) were co-added and converted into the frequency domain by a fast Fourier transformation, with the resulting frequency resolution of 25 kHz, full width half maximum (FWHM) of ~50 kHz, and accuracy of about 15 kHz in frequency measurement. For both 8–13 and 13-18 GHz, 4.5 million FIDs were co-added (each collected for 20 μs) and converted into the frequency domain by applying a fast Fourier transformation, yielding a frequency resolution of ~50 kHz, FWHM of ~100 kHz, and a frequency accuracy of about 20 kHz. Complete details of the design and characterization of the spectrometer are provided elsewhere (Schmitz et al., 2012; Pérez et al., 2016; Fatima et al., 2020).

The spectrum across 18-26 GHz was recorded using the K-band spectrometer, which uses the segmented approach (Fatima et al., 2020); (Neill et al., 2013). The bandwidth of 8 GHz is divided into 800 MHz segments, which are then concatenated together to produce a spectrum across the whole bandwidth. Similar to the COMPACT spectrometer, this instrument uses a fast-frame set-up of several excitation-detection cycles per molecular gas pulse. The AWG synthesizes 1.5 μs of excitation pulses in the range of 7-3 GHz; these chirps are then frequency upconverted to 9-13 GHz and doubled to 18-26 GHz. For each gas pulse, the molecular ensemble is polarized by a series of three pulse trains. The multi-train setup was performed simultaneously with a gas pulse repetition rate of 10 Hz, giving an effective repetition rate of 30 Hz. The FIDs were collected (each for 10 μs), frequency down-converted, co-added, and converted into the frequency domain by fast Fourier transformation. For this experiment, a total of 2.5 million acquisitions were recorded, with a resolution of ~100 kHz and FWHM of ~240 kHz. Complete details of the instrument are given in reference (Fatima et al., 2020).

Unlike the COMPACT and the K-band spectrometer, the spectrum was recorded at room temperature conditions in the W-band spectrometer. The experiment was set up in a slow flow cell condition in order to maintain a constant pressure inside the vacuum chamber. The liquid sample was heated to 55 °C resulting in a constant pressure of 1.5 mTorr in the spectrometer chamber. The instrument works with the segmented approach in which the 35 GHz bandwidth was covered in segments of 720 MHz each. For this experiment the High Dynamic Range (HDR) mode was used, which addresses each segment of 720 MHz by 30 chirps of 24 MHz spectral width each to reduce the spurious content in the measured spectrum (Arenas et al., 2017). The AWG synthesizes the excitation pulse in the 1.5-2.3 GHz range, which is then frequency upconverted and multiplied through a series of mixing stages and an active multiplier chain (x6) to produce the radiation in the millimeter-wave regime. Excitation pulses of 500 ns in duration were employed for this experiment. A total of one million FIDs (each recorded for 4 μs) were collected followed by conversion into the frequency domain by fast Fourier transformation. The achieved frequency accuracy of the instrument is ~30 kHz, with observed linewidths of ~550 kHz (Arenas et al., 2017) and a resolution of ~250 kHz under the conditions of the present experiment.

For all the experiments discussed above, the sample of MCA (>97% purity, purchased from Sigma Aldrich) was used without any further purification. A summary of the frequency ranges and the experimental conditions is collected in Supplementary Table S2.

The initial spectral analysis of the rotational spectra of MCA was done using the PGOPHER program (Western, 2017). The final fitting of the rotational parameters was achieved by using the XIAM program (Hartwig and Dreizler, 1996) for the simultaneous fitting of the A and E states for the parent species. For the assignment of the singly substituted ^{13}C and ^{15}N isotopologues in natural abundance, the SPFIT/SPCAT suite of programs (Pickett, 1991) was used to fit the A state transitions. The r_s structure analysis was performed with the KRA program package, followed by the calculation of the bond lengths and angles using the EVAL program. The effective structure $r_m^{(1)}$ was performed with the STRFIT program. All of these programs are available on the PROSPE website (PROSPE, 2022). The AABS package (Kisiel et al., 2005; PROSPE, 2022) was used for displaying the predicted transitions and measuring the experimental frequencies.

Results and discussion

The structures and principal axes for MCA_1 and MCA_2 are shown in Figure 1. Both conformers have a near prolate symmetry, as depicted by the values of Ray's asymmetry parameter, κ:

$$\kappa = \frac{2B - A - C}{A - C}$$

The experimentally obtained value of κ is -0.75 for MCA_1 and -0.96 for MCA_2.

Note that MCA_1 consists of an enantiomeric pair where the cyano group is rotated out of the plane of the ester fragment by ±20°. The interconversion pathway between the two enantiomers is essentially barrierless, as the calculated vibrational ground state lies above the calculated interconversion transition state at the B3LYP-D3/aug-cc-pVTZ level of theory, as shown in Supplementary Figure S2. The interconversion pathway of MCA_1 is also discussed in detail by Gregory et al. (Gregory et al., 2021). From the dihedral scan around NC-CH$_2$-C=O, the barrier height between MCA_1 and MCA_2 was found to be ~2 kJ/mol (170 cm^{-1}), as shown in Supplementary Figure S2.

For both conformers of MCA, the spectra recorded with the COMPACT and the K-band spectrometers show resolvable fine structure due to internal rotation and hyperfine structure (HFS)

TABLE 2 Experimental and theoretical rotational parameters for the two observed conformers of MCA. The theoretical rotational parameters were obtained at the B3LYP-D3/aug-cc-pVTZ level of theory.

	MCA_1			MCA_2	
Rotational parameters	Experiment (This work)	Previous study (Gregory et al., 2021)	Theory	Experiment (This work)	Theory
A^a/MHz	5069.2812(13)[h]	5069.2803(10)	5077	9429.0621(20)	9509
B/MHz	1842.95598(29)	1842.95524(23)	1830	1413.55699(12)	1407
C/MHz	1383.81701(17)	1383.81674(17)	1368	1249.82319(12)	1244
D_J^b/kHz	0.5057(18)	0.5087(19)	0.13	0.1363(42)	0.11
D_{JK}/kHz	1.074(38)	1.102(12)	6.64	−0.46472(26)	4.09
D_K/kHz	4.50(13)	[2.07]	10.25	12.24(47)	9.63
d_1/kHz	−0.17502(95)	−0.1769(20)	−0.02	−0.020225(30)	0.03
d_2/kHz	−0.04112(25)	−0.0458(14)	−0.03	−0.001776(37)	0.00
χ_{aa}^c/MHz	−1.1936(60)	−1.1924(24)	−1.39	−2.9569(53)	−3.38
χ_{bb-cc}/MHz	−2.767(10)	−2.7648(12)	−3.23	−1.103(10)	−1.23
V_3^d/kJ·mol^{-1}	4.4822(20)	4.579(6)	4.5[i]	4.7909(7)	4.6[i]
F_0^e/GHz	161.7128	160.34(22)	-	159.8404	-
δ^f/rad	0.4745(35)	0.4829(7)	-	2.6672(20)	-
σ^g/kHz	45	2.4	-	44	-
No. of lines	794	153	-	1580	-
Max J/K_a	39/4	6/3	-	43/27	-

[a]A, B, and C are the rotational constants.
[b]D_J, D_{JK}, D_K, d_1, and d_2 are the quartic centrifugal distortion constants.
[c]χ_{aa}, χ_{bb}, and χ_{cc} represent the diagonal elements of the ^{14}N nuclear quadrupole coupling tensor.
[d]V_3 is the potential barrier in a three-fold methyl internal rotation top.
[e]F_0 is the rotational constant of the methyl top.
[f]δ is the angle between the internal rotation axis and the a-axis.
[g]Microwave root-mean-square deviation of the fit.
[h]Statistical uncertainties are given in parentheses in units of the last digit.
[i]Theoretical potential barrier to the methyl internal rotation computed at the MP2/aug-cc-pVTZ level of theory.

due to nuclear quadrupole coupling. Each rotational transition is split into A and E components due to the internal rotation of the methyl group, and it is further split due to the interaction of the nuclear spin, I (^{14}N) = 1, with the electric field gradient. The pattern and the span of the splitting for one of the transitions can be clearly seen in the Figure 3, where a section of the rotational spectrum is shown together with the simulated spectra employing the fitted constants for MCA_1 and MCA_2.

The comprehensive analysis of the above-mentioned effects on the rotational spectra allowed us to effectively determine the nuclear quadrupole coupling constants for ^{14}N and the experimental barrier height (V_3) for the methyl internal rotor for both conformers of MCA. The comparison between the experimental and theoretical rotational constants is shown in Table 2. The two sets of rotational constants agree well within less than 1%. The comparison is further extended to the previous rotational spectroscopy study done on MCA_1 (Gregory et al., 2021). In the present work, more than 600 new transitions are added to the existing line list of MCA_1 while extending the probed J quantum number up to 39 in comparison to J = 6 as reported in reference (Gregory et al., 2021).

The set of experimentally determined rotational parameters given in Table 2 are obtained from the global fit (combined fit for the low and high frequency dataset) for each of the conformers, including the transitions between 2 and 110 GHz. The data were fit to a Watson S reduction Hamiltonian in an I^r representation. The XIAM software (Hartwig and Dreizler, 1996) was used for the fitting procedure as it can yield the barrier height (V_3) of the methyl internal rotation and nuclear quadrupole coupling constants simultaneously. The experimentally obtained barrier heights (4.4822(20) kJ/mol for MCA_1 and 4.7909(7) kJ/mol for MCA_2) are closer to the value predicted using MP2/aug-cc-pVTZ (4.5 kJ/mol for MCA_1 and 4.6 kJ/mol for MCA_2) as compared to the ones predicted using B3LYP-D3/aug-cc-pVTZ (3.2 kJ/mol for MCA_1 and 3.2 kJ/mol for MCA_2). In the XIAM fit, the internal rotation parameter, ε, was fixed to zero. ε is the angle between the projection of the methyl axis onto the bc-plane and the b-axis, but as the molecule lies in the ab-inertial plane, it makes the methyl internal rotation axis and b-axis coplanar, as shown in Figure 1.

In the high frequency region (75-110 GHz), the HFS is not resolved as the splitting collapses with increase in the J
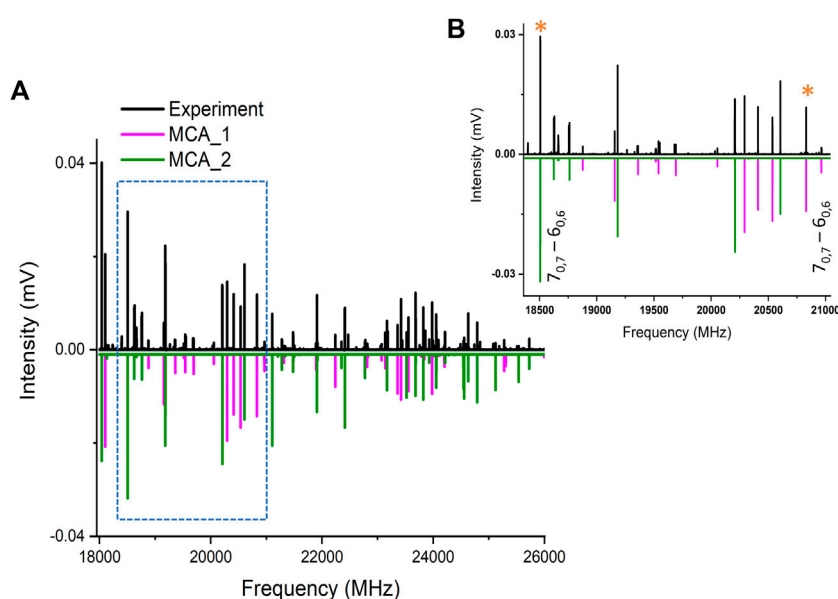
FIGURE 2
Panel **(A)** shows the rotational spectrum of MCA recorded with the *K*-band spectrometer in the 18-26 GHz region. The upper black trace is the experimental spectrum, the lower colored traces are the simulated spectra based on the fitted rotational constants at 3 K for both conformers of MCA (MCA_1 in magenta and MCA_2 in green). The zoom-in (panel **(B)**) illustrates the assignment and the intensity ratio of the two conformers. The rotational transition $J_{Ka,Kc}-J'_{Ka',Kc'} = 7_{0,7}-6_{0,6}$ is marked with an asterisk to highlight the difference in intensities for MCA_1 and MCA_2. Note that the transition intensities in different parts of the spectrum can be influenced by frequency-dependent instrumental effects, such as the amplifier performances.

quantum number. Hence the nuclear quadrupole coupling constants were determined from the low-frequency dataset alone. To obtain a global fit across all covered
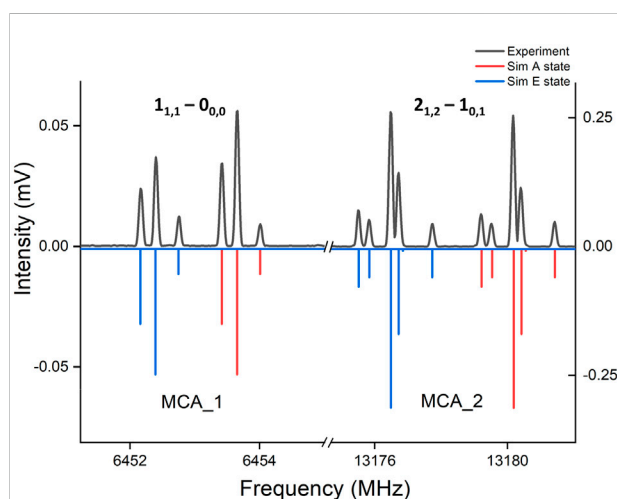

FIGURE 3
The upper trace shows a part of the experimental rotational spectrum of MCA, highlighting the internal rotation splitting (red and blue) followed by the splitting due to nuclear quadrupole coupling. The bottom trace shows the simulation based on the fitted rotational constants.

frequency regions, the transitions with resolved HFS and transitions with unresolved HFS were included together in the same line list. In the high frequency region, for each rotational transition with unresolved HFS we assigned the three most intense HFS components to the same experimental frequency without increasing the uncertainty for these merged transitions.

In addition to the XIAM fit, fits including only the A-state transitions for both MCA_1 and MCA_2 were performed with the SPFIT/SPCAT suite of programs (Pickett, 1991) for the astronomical searches in different regions of the ISM. The experimental rotational parameters obtained for both conformers are given in Supplementary Tables S3,S4. The line list contains the assigned experimental frequencies together with their uncertainties. The .cat files generated with the SPCAT program contain predicted transition frequencies up to 150 GHz based on the fitted rotational parameters. The predicted uncertainties for transitions up to 150 GHz are predominantly less than 1 MHz and therefore should be highly reliable for the search of MCA in the ISM. For instance, there are more than 250 transitions for MCA_1 and more than 2000 transitions for MCA_2 with uncertainties below 40 kHz in the frequency range of 84-116 GHz (ALMA Band 3).
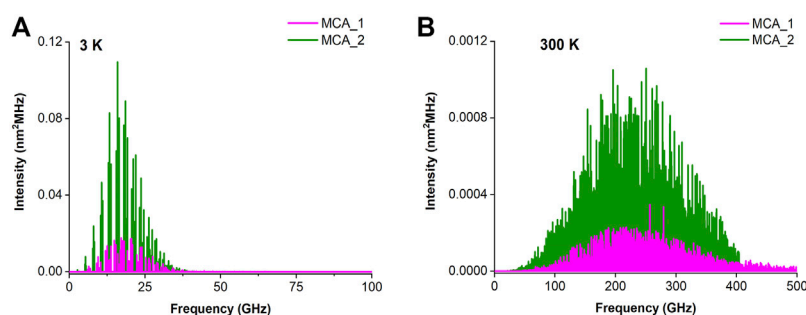
FIGURE 4
The distribution of the rotational transitions of MCA_1 (magenta) and MCA_2 (green) at 3 K (left, panel **(A)**) and at 300 K (right, panel **(B)**). The spectra were simulated up to 500 GHz and J quantum numbers up to 100. The plot was made for the case of $2I+1 = 1$, considering only a-type transitions. Note the different intensity scales for the two panels.

TABLE 3 Rotational partition function (Q_{rot}) calculated across the standard temperatures implemented in the JPL database (Pickett et al., 1998).

T/K	MCA_1		MCA_2	
	Q_{rot} [2I+1=1][a]	Q_{rot} [2I+1 = 3][b]	Q_{rot} [2I+1 = 1][a]	Q_{rot} [2I+1 = 3][b]
300	130946.98	392806.84	109601.70	328691.10
225	104461.39	313353.30	86967.91	260811.73
150	70438.51	211294.93	59020.07	177000.75
75	29606.48	88819.47	25600.40	76785.97
37.5	10768.97	32309.45	9470.87	28411.75
18.75	3811.79	11435.85	3356.85	10070.55
9.375	1349.12	4047.43	1188.08	3564.25
1.5	87.42	262.25	76.90	230.69

[a]$I = 0$, assuming no hyperfine structure.
[b]$I = 1$, considering hyperfine structure.

Rotational partition function and transition intensities for MCA_1 and MCA_2

To facilitate the astronomical searches for MCA, in addition to providing accurate rest frequencies for the two assigned conformers, information on the relative intensities of the rotational transitions at different temperatures is calculated from the rotational partition function. The rotational partition function, Q_{rot}, represents the accessible rotational energy states at a given temperature for a molecule. For an asymmetric top, it is approximated as

$$Q_{rot} = 5.3311 \times 10^6 \left(\frac{T^3}{ABC} \right)^{\frac{1}{2}} \Big/ \sigma \qquad (1)$$

where σ is the symmetry parameter, T the sample temperature (K), and A, B, and C the rotational constants of the molecule (MHz) (Gordy and Cook, 1984). The rotational partition function can be useful for calculating absorption coefficients and hence the transition intensities, which can be further used for the calculation of column densities of the species of interest (Mangum and Shirley, 2015).

As Q_{rot} depends on the temperature, changing the temperature results in a change of the intensity distribution of the observed rotational transitions. This can be seen in Figure 4, which shows the simulated spectra for MCA_1 and MCA_2 based on their μ_a dipole-moment components and calculated partition functions at 3 and 300 K, respectively. In the present work, Q_{rot} is calculated for two nuclear spin states, $I = 0$, spin degeneracy $2I+1 = 1$, where hyperfine structure is not considered, and for $I = 1$, spin degeneracy $2I+1 = 3$, considering the hyperfine structure caused by nitrogen with I (^{14}N) = 1, as shown in Table 3. The rotational partition function is calculated for the A state transitions of both MCA_1 and MCA_2, across standard temperatures, as implemented in the JPL database (Pickett et al., 1998).

The rotational transition intensities are proportional to the product of $\mu^2 \cdot N_i$, μ being the dipole-moment component

associated with the transition, and N_i being the fraction of molecules in the ground state of that transition. MCA_1 and MCA_2 can be considered to be essentially isoenergetic, although all our quantum-chemical calculations predict MCA_2 to be slightly higher in energy than MCA_1. However, the substantially higher dipole-moment component of MCA_2 compensates for it. In general, the observed a-type transitions for MCA_2 are of similar intensity or are more intense than those for MCA_1, as μ_a is 2.3 D for MCA_1, while μ_a is 4.5 D for MCA_2. In Figure 2, the rotational spectrum recorded in 18-26 GHz is shown. Panel B highlights the intensity difference observed for MCA_1 and MCA_2 (marked by an asterisk) for the rotational transition $7_{0,7} – 6_{0,6}$. Note that these marked transitions are ~2.5 GHz apart, so that instrumental effects, such as the frequency dependencies of the horn antennas and the amplifier gains, can influence the absolute intensity. However, the overall higher intensity of rotational transitions for MCA_2 compared to MCA_1 has been observed in our experiments, especially in the W-band region (75-110 GHz). This observation is supported by the total number of assigned transitions. For MCA_1, a total of 794 transitions were assigned with a J quantum number up to 39 in comparison to 1580 assigned transitions for MCA_2 with a J quantum number up to 43, shown in the Table 2.

Interstellar search towards the G+0.693-0.027 molecular cloud

We conducted a search for both conformers of MCA using a high sensitivity spectral survey carried out towards the G+0.693-0.027 molecular cloud (hereafter G+0.693), located in the Sgr B2 region of the Galactic Center. This region is one of the most chemically rich sources in the ISM, including many species with the cyano group (-C≡N) (Rivilla et al., 2022a), such as cyanoacetylene (HC$_3$N), acetonitrile (CH$_3$CN), cyanamide (NH$_2$CN), the cyanomethyl and the cyanomidyl radicals (H$_2$CCN and HNCN, respectively), C-cyanomethanimine (HNCHCN), cyanic acid (HOCN), and glycolonitrile (HOCH$_2$CN) (Zeng et al., 2018; Rivilla et al., 2019; Rodríguez-Almeida et al., 2021; Rivilla et al., 2022b). This makes G+0.693 a suited interstellar source to search for MCA.

We used the IRAM 30 m telescope (Granada, Spain) and the Yebes 40 m telescope (Guadalajara, Spain). The observations were centred at α(J2000.0) = 17h47m22s, and δ(J2000.0) = −28∘21′27″. The position switching mode was used in all the observations with the off position located at Δα = −885″, Δδ = 290" from the source position. In this work, we have used data covering the spectral windows from 31.3 GHz to 50.6 GHz (Yebes telescope) and from 71.8 to

116.7 GHz (IRAM 30 m telescope). The line intensity of the spectra was measured in units of T_A^* (antenna temperature as a scale) as the molecular emission toward G+0.693 is extended over the beam (Requena-Torres et al., 2006; Requena-Torres et al., 2008; Zeng et al., 2018; Zeng et al., 2020). More details about the observations can be found in references (Rivilla et al., 2021; Rodríguez-Almeida et al., 2021).

MCA was searched for in the observational data using the SLIM (Spectral Line Identification and Modelling) tool within the MADCUBA package[3] (version 11/03/2022) (Martín et al., 2019). The rotational spectroscopy data for the A state transitions presented in this work was implemented into the SLIM tool, which enabled us to generate the synthetic spectra of both conformers of MCA under the assumption of Local Thermodynamic Equilibrium (LTE).

None of the MCA conformers were detected towards the G+0.693 molecular cloud. Therefore, we have computed upper limits for their molecular column densities (N) using the brightest transitions according to the synthetic LTE model generated by SLIM. We used typical values for the physical parameters: excitation temperature, T_{ex} = 10 K, full width half maximum, FWHM = 10 km s^{-1}, and velocity, v_{LSR} = 69 km s^{-1}. The brightest transitions predicted by the LTE model within the spectral survey are the $12_{0,12}–11_{0,11}$ transitions, at 34.528700 GHz (E_{up} = 11.01 K) and at 31.320023 GHz (E_{up} = 9.78 K) for MCA_1 and MCA_2, respectively. Figure 5 shows the observed spectrum around these frequencies, where no clear line emission is detected. We measured a noise level (σ) in the velocity range of ±300 km s^{-1} around these transitions (Figure 5) of 1.5 and 2.7 mK for MCA_1 and MCA_2, respectively. We derived the column density upper limits (A states) of <1.2 × 10^{13} cm^{-2} for MCA_1 and <0.4 × 10^{13} cm^{-2} for MCA_2, using the 3σ value of the integrated intensity, see further details in reference (Martín et al., 2019). Using the column density of molecular hydrogen, N(H$_2$) = 1.35 × 10^{23} cm^{-2}, the molecular abundances (A states) were derived to be < 9 × 10^{-11} and <3 × 10^{-11} for MCA_1 and MCA_2, respectively. Despite the noisier spectrum around the MCA_2 transitions, the most stringent upper limit was obtained for this higher energy conformer, due to its larger dipole moment. Note that since we only focus on the A state transitions here, the actual upper limits for the abundances of MCA_1 and MCA_2 can be expected to be somewhat higher than the values reported here.

MCA is a complex organic molecule with twelve atoms, containing seven heavy atoms, namely, four carbon (C), two oxygen (O), and one nitrogen (N) atoms. So far, the most complex CON-bearing species detected in the ISM are ethyl isocyanate (CH$_3$CH$_2$NCO) (Rodríguez-Almeida et al., 2021) and ethanolamine (NH$_2$CH$_2$CH$_2$OH) (Rivilla et al., 2021), both detected towards G+0.693. These two molecules are somewhat
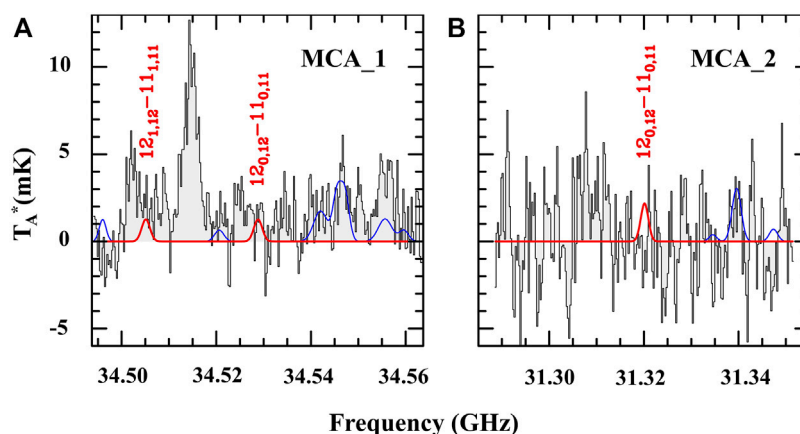

3　https://cab.inta-csic.es/madcuba/

FIGURE 5
The brightest transitions of MCA_1 (panel **(A)**) and MCA_2 (panel **(B)**) according to the Local Thermodynamic Equilibrium (LTE) towards the G+0.693-0.027 molecular cloud. The synthetic spectrum (red solid line) is derived using the upper limits to the column densities for the typical parameters (T_{ex}, FWHM, and V_{LSR}) found in this source, as outlined in the text. The black solid line and gray histogram correspond to the observed spectra towards the source. The blue solid line shows the contribution from other molecular species already identified in the spectral survey.
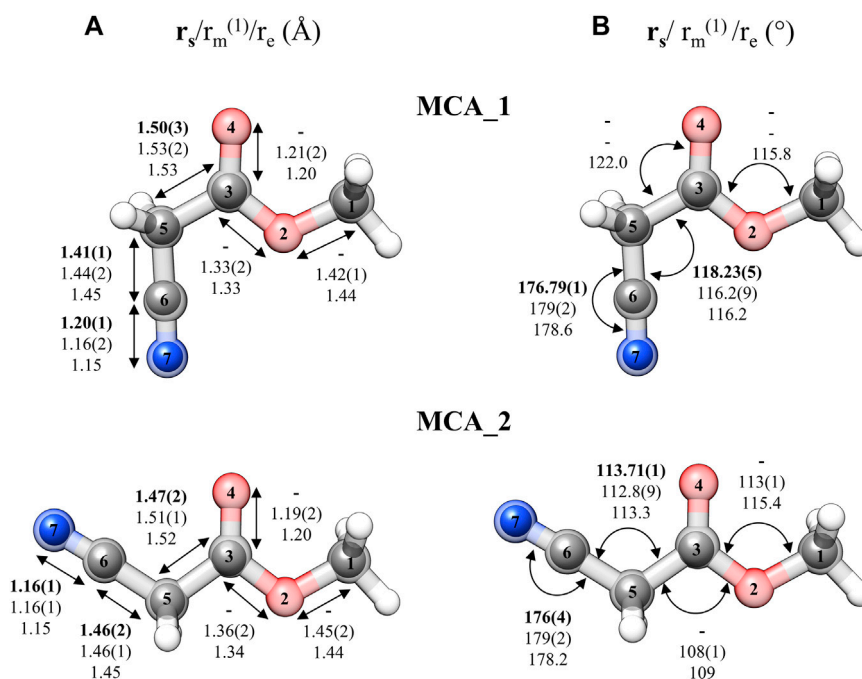

FIGURE 6
The experimental structures of MCA_1 and MCA_2. The inner bold spheres represent the r_s positions of the atoms, whereas the partially transparent backbone gives the theoretical r_e structures (B3LYP-D3/aug-cc-pVTZ level of theory). The bond distances (panel **(A)**) and angles (panel **(B)**) obtained by the three methods, r_s, $r_m^{(1)}$, and r_e, are also included where applicable.

lighter than MCA, since they contain ten and eleven atoms, respectively, and only four heavy atoms. The abundances found for ethyl isocyanate and ethanolamine are ~(0.5–1.5) x 10^{-10}.

The upper limits of the A states of two MCA conformers derived in this work are <(0.3–0.9) x 10^{-10}, i.e., similar to the abundances of the simpler CON-species ethyl isocyanate and

ethanolamine. Since MCA is a more complex molecule, it is not surprising that its abundance in the ISM is lower. This is in good agreement with the observed general trend of decreasing abundances with increasing chemical complexity found for several chemical families (Zeng et al., 2018), (Jiménez-Serra et al., 2019), (Sanz-Novo, 2022). Therefore, to detect more complex species such as MCA, and to study the growth of chemical complexity in the ISM, deeper observations with higher sensitivities are needed, which will allow us to address the detection of complex species with abundances $<10^{-11}$.

Structure determination

Due to the high signal-to-noise ratio for the two conformers in the 2-26 GHz frequency range, we were able to assign the rotational spectra of the singly substituted ^{13}C and ^{15}N isotopologues in natural abundances of 1.1 and 0.4%, respectively. The experimentally obtained rotational parameters are given in the Supplementary Tables S3,S4. From this information, we could determine the structures of the two conformers of MCA using the substitution structure and the effective structure methods.

Kraitchman's substitution method, r_s (Kraitchman, 1953), exploits changes in the moments of inertia upon single isotopic substitution. This approach allows us to unambiguously determine the coordinates of each isotopically substituted atom in the principal inertial axis frame (the signs can be assigned from the theoretical or effective structure coordinates). Another way to exploit the single-isotopic information is to obtain the bond distances and angles from a least-squares fit of all the available rotational parameters. This method allows us to determine a total or partial effective ground state r_0 structure (Kisiel, 2003). In our analysis, we employed the $r_m^{(1)}$ method (Watson et al., 1999), as it incorporates additional terms that account for vibration - rotation corrections, which are not considered in the r_s and r_0 methods. The results of the application of the r_s and $r_m^{(1)}$ methods given in the Supplementary Tables S5–S8 are summarized in Figure 6, where they show the good consistency between experimental and theoretical data.

One of the drawbacks from the Kraitchman's method is that it frequently gives imaginary values for some coordinates if they are close to zero. In the case of MCA, most of the c coordinates for the atoms are close to zero since they lie almost directly on the ab-inertial plane. As a result of this, we kept the c coordinates fixed to zero giving rise to a planar r_s structure. The values of the planar moments of inertia P_{cc} (4.3519(1) amu·Å^2 for MCA_1 and 3.03803(1) amu·Å^2 for MCA_2) suggest the ground state structure to be near planar, with the -CN group slightly tilted with respect to the ab-inertial plane. This is also supported by the equilibrium structure r_e obtained from the theoretical calculations performed at the B3LYP-D3/aug-cc-pVTZ level of theory.

Figure 6 shows the overlay of the experimentally obtained r_s and $r_m^{(1)}$ structures (in bold spheres) and the theoretical structure, obtained at the B3LYP-D3/aug-cc-pVTZ level of theory (partially transparent back bone) for both MCA_1 and MCA_2. The structure of MCA can be compared with a similar molecule, cyanoacetic acid (Sanz-Novo et al., 2021), as MCA is a methyl ester of cyanoacetic acid. The most stable conformer of cyanoacetic acid is the *cis* configuration of the -CN group with respect to the carbonyl oxygen. This arrangement corresponds to MCA_2 in our study, while, in the most stable configuration of MCA (MCA_1), the -CN group is *gauche* with respect to the carbonyl group. This can be attributed to the combination of the attractive forces between the H atoms of the methyl rotor and the carbonyl carbon and the lone pair of electrons on the ester oxygen and the carbon of the CN-group, as discussed thoroughly in reference (Gregory et al., 2021), making the conformation of MCA_1 slightly more stable.

Conclusion

We present an extensive laboratory study of the rotational spectra of the two lowest energy conformers of MCA in which the internal rotation and nuclear quadrupole coupling splittings have been resolved. We report the detailed characterization of MCA_2, which has not been investigated before, while extending the previous microwave investigation for MCA_1 into the millimeter wave region. The final analysis comprises of the assignment of rotational transition frequencies between 2-26 GHz and 75-110 GHz and the precise determination of the rotational parameters up to the quartic centrifugal distortion constants, including the internal rotation barrier (V_3) of the methyl group and the nitrogen nuclear quadrupole coupling constants, for both conformers of MCA. In addition, the assignments in the high-frequency data set lead to the accurate determination of the centrifugal distortion constants, which in turn allowed us to compute reliable rest frequencies up to 150 GHz, with line uncertainties clearly below 1 MHz for most of the predicted transitions. Precisely, more than 250 transitions for MCA_1 and more than 2000 transitions for MCA_2 are predicted with accuracies better than 0.1 km/s (<40 kHz) in the frequency range of ALMA Band 3. We also provide precise structural information for both MCA_1 and MCA_2.

One of the notable results from this study is that despite the fact that MCA_2 is slightly higher in energy than MCA_1, the intensities of MCA_2 are generally observed to be more intense than those of MCA_1, owing to the higher value of the electric dipole moment of MCA_2. The number of assigned transitions especially in the higher frequency region, where MCA_1 can scarcely be seen while MCA_2 dominates the rotational spectrum, further supports this finding. This result is of great interest as it emphasizes the need to also consider higher-energy

conformers as promising candidates for interstellar detection, especially in the warmer regions of the ISM, since at elevated temperatures, the higher energy conformers are expected to be more populated as compared to the colder regions. Based on our results, MCA_2 is a more favorable conformer of MCA to be detected in the ISM.

Using the precise spectral predictions based on our laboratory spectra, a search for both MCA_1 and MCA_2 was attempted towards the G+0.693 molecular cloud located in the Sgr B2 region of the Galactic Centre. None of the MCA conformers were detected. We derived a column density upper limit of $<1.2 \times 10^{13}$ cm^{-2} for MCA_1 and $<0.4 \times 10^{13}$ cm^{-2} for MCA_2, based on the A state predictions. Such a comprehensive study, which covers the assignment of the rotational transitions in the low and high frequency regime, is essential for interstellar searches, as the large frequency range allows the experimental transition frequencies to be directly compared with the observational spectra. For example, the data in the 2-26 GHz range can be used for searches using the Effelsberg telescope and the line frequencies in 75-110 GHz can be directly compared with the observational data from the Atacama Large Millimeter Array Band 3. The detection of two conformers of MCA in the ISM will be a step forward in the direction of increasing structural complexity of the molecules present in the ISM.

Data availability statement

The original contributions presented in the study are included in the article/Supplementary Material. Further inquiries can be directed to the corresponding author.

Author contributions

GB: Conceptualization, experimentation, Formal analysis, Investigation, Data analysis, Writing—original draft, Writing—review and editing, Project administration. PP: Formal analysis, Investigation, Data analysis, Writing—original draft, Writing—review and editing. AS: Conceptualization, Investigation, Writing—review and editing. VR, IJ-S, and JM-P: Astronomical data analysis, Writing—review and editing. MS: Resources, Writing—review and editing, Supervision, Funding acquisition, Project administration.

Funding

Acknowledgments

Conflict of interest

The authors declare that the research was conducted in the absence of any commercial or financial relationships that could be construed as a potential conflict of interest.

The reviewer MM declared a past collaboration with several of the authors VR, IJ-S, AND JM-P to the handling editor.

Publisher's note

All claims expressed in this article are solely those of the authors and do not necessarily represent those of their affiliated organizations, or those of the publisher, the editors and the reviewers. Any product that may be evaluated in this article, or claim that may be made by its manufacturer, is not guaranteed or endorsed by the publisher.

Supplementary material

The Supplementary Material for this article can be found online at: https://www.frontiersin.org/articles/10.3389/fspas.2022.977488/full#supplementary-material

References

Arenas, B. E., Gruet, S., Steber, A. L., Giuliano, B. M., and Schnell, M. (2017). Chirped-pulse fourier transform millimeter-wave spectroscopy of ten vibrationally excited states of i-propyl cyanide: Exploring the far-infrared region. *Phys. Chem. Chem. Phys.* 19, 1751–1756. doi:10.1039/C6CP06297K

Biver, N., Bockelée-Morvan, D., Moreno, R., Crovisier, J., Colom, P., Lis, D.C., et al. (2015). Ethyl alcohol and sugar in comet C/2014 Q2 (Lovejoy). *Sci. Adv.* 1, e1500863. doi:10.1126/sciadv.1500863

Brown, G. G., Dian, B. C., Douglass, K.O., Geyer, S. M., and Pate, B. H. (2006). The rotational spectrum of epifluorohydrin measured by chirped-pulse Fourier transform microwave spectroscopy. *J. Mol. Spectrosc.* 238, 200–212. doi:10.1016/j.jms.2006.05.003

Charles, S.W., Jones, G. I. L., and Owen, N. L. (1973). Vibrational spectra and rotational isomerism of methyl and ethyl cyanoacetate. *J. Chem. Soc. Faraday Trans. 2* 269, 1454. doi:10.1039/f29736901454

Despois, D., Biver, N., Bockelée-Morvan, D., and Crovisier, J. (2006). Observations of molecules in comets. *Proc. Int. Astron. Union* 1, 469. doi:10.1017/S1743921306007484

Fatima, M., Pérez, C., Arenas, B. E., Schnell, M., and Steber, A. L. (2020). Benchmarking a new segmented K-band chirped-pulse microwave spectrometer and its application to the conformationally rich amino alcohol isoleucinol. *Phys. Chem. Chem. Phys.* 22, 17042–17051. doi:10.1039/D0CP01141J

Frisch, M. J., Trucks, G. W., Schlegel, H. B., Scuseria, G. E., Robb, M. A., Cheeseman, J. R., et al. (2013). *Gaussian 09 Citation*. Wallingford CT: Gaussian, Inc.. Revision D.01(n.d.).

Gordy, W., and Cook, R. L. (1984). *Microwave molecular spectra*. New York: Wiley.

Gregory, C., Silva, W. G. D. P., and van Wijngaarden, J. (2021). Rotational spectrum and quantum chemical calculations of methyl cyanoacetate: A compound of potential astrochemical interest. *J. Mol. Spectrosc.* 377, 111444. doi:10.1016/j.jms.2021.111444

Hartwig, H., and Dreizler, H. (1996). The microwave spectrum of trans-2, 3-dimethyloxirane in torsional excited states. *Z. Für Naturforsch. A* 51, 923–932. doi:10.1515/zna-1996-0807

Herbst, E., and van Dishoeck, E. F. (2009). Complex organic interstellar molecules. *Annu. Rev. Astron. Astrophys.* 47, 427–480. doi:10.1146/annurev-astro-082708-101654

Jiménez-Serra, I., Martín-Pintado, J., Insausti, A., Alonso, E. R., Cocinero, E. J., and Bourke, T. L. (2009). "The SKA as a Prebiotic Molecule Detector," in *Frontiers in Astronomy and Space Sciences* 9 (Accessed June 20, 2022. doi:10.3389/fspas.2022.843766)

Kisiel, Z. (2003). Least-squares mass-dependence molecular structures for selected weakly bound intermolecular clusters. *J. Mol. Spectrosc.* 218, 58–67. doi:10.1016/S0022-2852(02)00036-X

Kisiel, Z., Pszczółkowski, L., Medvedev, I. R., Winnewisser, M., DeLucia, F.C., and Herbst, E. (2005). Rotational spectrum of trans–trans diethyl ether in the ground and three excited vibrational states. *J. Mol. Spectrosc.* 233, 231–243. doi:10.1016/j.jms.2005.07.006

Kleiner, I. (2019). Spectroscopy of interstellar internal rotors: An important tool for investigating interstellar chemistry. *ACS Earth Space Chem.* 3, 1812–1842. doi:10.1021/acsearthspacechem.9b00079

Kraitchman, J. (1953). Determination of molecular structure from microwave spectroscopic data. *Am. J. Phys.* 21, 17–24. doi:10.1119/1.1933338

Leibowitz, S. J., Laane, J., Van Alsenoy, C., and van der Veken, B. J. (1991). On the conformational analysis of methyl cyanoacetate. *J. Mol. Struct.* 248, 251–273. doi:10.1016/0022-2860(91)80035-3

Mangum, J. G., and Shirley, Y. L. (2015). How to calculate molecular column density. *Publ. Astron. Soc. Pac.* 127, 266–298. doi:10.1086/680323

Martín, S., Martín-Pintado, J., Blanco-Sánchez, C., Rivilla, V. M., Rodríguez-Franco, A., and Rico-Villas, F. (2019). Spectral line identification and modelling (SLIM) in the Madrid data Cube analysis (MADCUBA) package: Interactive software for data cube analysis. *Astron. Astrophys.* 631, A159. doi:10.1051/0004-6361/201936144

McGuire, B. A. (2022). 2021 census of interstellar, circumstellar, extragalactic, protoplanetary disk, and exoplanetary molecules. *Astrophys. J. Suppl. Ser.* 259, 30. doi:10.3847/1538-4365/ac2a48

Neese, F. (2012). The ORCA program system. *WIREs Comput. Mol. Sci.* 2, 73–78. doi:10.1002/wcms.81

Neese, F. (2018). Software update: The ORCA program system, version 4.0. *WIREs Comput. Mol. Sci.* 8, 1327. doi:10.1002/wcms.1327

Neill, J. L., Harris, B. J., Steber, A. L., Douglass, K. O., Plusquellic, D. F., and Pate, B. H. (2013). Segmented chirped-pulse Fourier transform submillimeter spectroscopy for broadband gas analysis. *Opt. Express* 21, 19743. doi:10.1364/OE.21.019743

Neta, J. M. F., and Fausto, R. (1998). Molecular structure and vibrational spectra of methyl cyanoacetate: An FT-IR, Raman and *ab initio* molecular orbital study. *J. Mol. Struct.* 443, 41–56. doi:10.1016/S0022-2860(97)00361-X

Pearson, J. C., Sastry, K. V. L. N., Herbst, E., and Lucia, F. C. D. (1997). Gauche ethyl alcohol: Laboratory assignments and interstellar identification. *Astrophys. J.* 480, 420–431. doi:10.1086/303967

Pérez, C., Krin, A., Steber, A. L., López, J. C., Kisiel, Z., and Schnell, M. (2016). Wetting camphor: Multi-isotopic substitution identifies the complementary roles of hydrogen bonding and dispersive forces. *J. Phys. Chem. Lett.* 7, 154–160. doi:10.1021/acs.jpclett.5b02541

Pickett, H. M., Poynter, R. L., Cohen, E. A., Delitsky, M. L., Pearson, J. C., and Müller, H. S. P. (1998). Submillimeter, millimeter, and microwave spectral line catalog. *J. Quant. Spectrosc. Radiat. Transf.* 60, 883–890. doi:10.1016/S0022-4073(98)00091-0

Pickett, H. M. (1991). The fitting and prediction of vibration-rotation spectra with spin interactions. *J. Mol. Spectrosc.* 148, 371–377. doi:10.1016/0022-2852(91)90393-O

Prasad, R., Mishra, Y. K., and Gupta, R. K. (1990). Spectroscopic and molecular mechanics study of the conformational properties of methyl cyanoacetate and ethyl cyanoacetate. *Indian J. Chem.* 29A, 618–623.

PROSPE (2022). Programs for ROtational SPEctroscopy. Available at: http://www.ifpan.edu.pl/~kisiel/prospe.htm (accessed February 25, 2022).

Requena-Torres, M. A., Martín-Pintado, J., Rodríguez-Franco, A., Martín, S., Rodríguez-Fernández, N. J., and de Vicente, P. (2006). Organic molecules in the Galactic center - hot core chemistry without hot cores. *Astron. Astrophys.* 455, 971–985. doi:10.1051/0004-6361:20065190

Requena-Torres, M. A., Martin-Pintado, J., Martin, S., and Morris, M. R. (2008). The galactic center: The largest oxygen-bearing organic molecule repository. *Astrophys. J.* 672, 352–360. doi:10.1086/523627

Reva, I. D., Ilieva, S. V., and Fausto, R. (2001). Conformational isomerism in methyl cyanoacetate: A combined matrix-isolation infrared spectroscopy and molecular orbital study. *Phys. Chem. Chem. Phys.* 3, 4235–4241. doi:10.1039/b104671n

Reva, I. D., Stepanian, S. G., Adamowicz, L., and Fausto, R. (2003). Missing conformers. Comparative study of conformational cooling in cyanoacetic acid and methyl cyanoacetate isolated in low temperature inert gas matrixes. *Chem. Phys. Lett.* 374, 631–638. doi:10.1016/S0009-2614(03)00782-6

Rivilla, V. M., Beltrán, M. T., Martín-Pintado, J., Fontani, F., Caselli, P., and Cesaroni, R. (2017). On the chemical ladder of esters - detection and formation of ethyl formate in the W51 e2 hot molecular core. *Astron. Astrophys.* 599, A26. doi:10.1051/0004-6361/201628823

Rivilla, V. M., Martín-Pintado, J., Jiménez-Serra, I., Zeng, S., Martín, S., Armijos-Abendaño, J., et al. (2019). Abundant Z-cyanomethanimine in the interstellar medium: Paving the way to the synthesis of adenine. *Mon. Not. R. Astron. Soc. Lett.* 483, L114–L119. –L119. doi:10.1093/mnrasl/sly228

Rivilla, V. M., Jiménez-Serra, I., Martín-Pintado, J., Briones, C., Rodríguez-Almeida, L. F., Rico-Villas, F., et al. (2021). Discovery in space of ethanolamine, the simplest phospholipid head group. *Proc. Natl. Acad. Sci. U. S. A.* 118, e2101314118. doi:10.1073/pnas.2101314118

Rivilla, V. M., Jiménez-Serra, I., Martín-Pintado, J., Colzi, L., Tercero, B., de Vicente, P., et al. (2022a). Molecular precursors of the RNA-world in space: New nitriles in the G+0.693-0.027 molecular cloud Available at: http://arxiv.org/abs/2206.01053 (Accessed on June 20, 2022).

Rivilla, V. M., Colzi, L., Jiménez-Serra, I., Martín-Pintado, J., Megías, A., Melosso, M., et al. (2022b). Precursors of the RNA world in space: Detection of (Z)-1, 2-ethenediol in the interstellar medium, a key intermediate in sugar formation. *Astrophys. J. Lett.* 929, L11. doi:10.3847/2041-8213/ac6186

Rodríguez-Almeida, L.F., Rivilla, V. M., Jiménez-Serra, I., Melosso, M., Colzi, L., Zeng, S., et al. (2021). First detection of C2H5NCO in the ISM and search of other isocyanates towards the G+0.693-0.027 molecular cloud. *Astron. Astrophys.* 654, L1. doi:10.1051/0004-6361/202141989

Sanz-Novo, M., León, I., Alonso, E. R., Kolesniková, L., and Alonso, J. L. (2021). Laboratory detection of cyanoacetic acid: A jet-cooled rotational study. *Astrophys. J.* 915, 76. doi:10.3847/1538-4357/ac013f

Sanz-Novo, M. (2022). Toward the limits of complexity of interstellar chemistry: Rotationalspectroscopy and astronomical search for n- and i-butanal. Available at: https://www.frontiersin.org/article/10.3389/fspas.2022.843766 (Accessed June 20, 2022).

Schmitz, D., Alvin Shubert, V., Betz, T., and Schnell, M. (2012). Multi-resonance effects within a single chirp in broadband rotational spectroscopy: The rapid adiabatic passage regime for benzonitrile. *J. Mol. Spectrosc.* 280, 77–84. doi:10.1016/j.jms.2012.08.001

Sinha, D., and Katon, J.E. (1974). The vibrational spectra of methyl cyanoacetate and methyl cyanoacetate-d_3. *Can. J. Chem.* 52, 3057–3062. doi:10.1139/v74-448

Tercero, B., Kleiner, I., Cernicharo, J., Nguyen, H. V. L., López, A., and Caro, G. M. M. (2013). Discovery of methyl acetate and gauche ethyl formate in orion. *Astrophys. J.* 770, L13. doi:10.1088/2041-8205/770/1/L13

Walker, R. M., and Cameron, A. G. W. (2006). *Meteorites and the early solar system II*. University of Arizona Press. doi:10.2307/j.ctv1v7zdmm

Watson, J. K. G., Roytburg, A., and Ulrich, W. (1999). Least-squares mass-dependence molecular structures. *J. Mol. Spectrosc.* 196, 102–119. doi:10.1006/jmsp.1999.7843

Western, C. M. (2017). Pgopher: A program for simulating rotational, vibrational and electronic spectra. *J. Quant. Spectrosc. Radiat. Transf.* 186, 221–242. doi:10.1016/j.jqsrt.2016.04.010

Zeng, S., Jiménez-Serra, I., Rivilla, V. M., Martín, S., Martín-Pintado, J., Requena-Torres, M. A., et al. (2018). Complex organic molecules in the galactic Centre: The N-bearing family. *Mon. Not. R. Astron. Soc.* 478, 2962–2975. doi:10.1093/mnras/sty1174

Zeng, S., Zhang, Q., Jiménez-Serra, I., Tercero, B., Lu, X., Martín-Pintado, J., et al. (2020). Cloud–cloud collision as drivers of the chemical complexity in Galactic Centre molecular clouds. *Mon. Not. R. Astron. Soc.* 497, 4896–4909. doi:10.1093/mnras/staa2187

Zuckerman, B., Turner, B. E., Johns, D. R., Lovas, F. J., Fourikis, N., Palmer, P., et al. (1975). Detection of interstellar trans-ethyl alcohol. *Astrophys. J.* 196, L99. doi:10.1086/181753